Available online at www.sciencedirect.com
ScienceDirect
Composites Science and Technology 67 (2007) 3130–3139
COMPOSITES SCIENCE AND TECHNOLOGY
www.elsevier.com/locate/compscitech

Self-assembled natural rubber/silica nanocomposites: Its preparation and characterization

Zheng Peng [a,b,*], Ling Xue Kong [b], Si-Dong Li [c], Yin Chen [a], Mao Fang Huang [a]

[a] *Chinese Agricultural Ministry Key Laboratory of Natural Rubber Processing, Agricultural Product Processing Research Institute at Chinese Academy of Tropical Agricultural Sciences, Zhanjiang 524001, China*
[b] *Centre for Advanced Manufacturing Research, University of South Australia, Mawson Lakes SA 5095, Australia*
[c] *College of Science, Guangdong Ocean University, Zhanjiang 524088, China*

Received 30 October 2006; received in revised form 4 April 2007; accepted 26 April 2007
Available online 22 May 2007

Abstract

A novel natural rubber/silica (NR/SiO_2) nanocomposite is developed by combining self-assembly and latex-compounding techniques. The results show that the SiO_2 nanoparticles are homogenously distributed throughout NR matrix as nano-clusters with an average size ranged from 60 to 150 nm when the SiO_2 loading is less than 6.5 wt%. At low SiO_2 contents ($\leqslant$4.0 wt%), the NR latex (NRL) and SiO_2 particles are assembled as a core-shell structure by employing poly (diallyldimethylammonium chloride) (PDDA) as an inter-medium, and only primary aggregations of SiO_2 are observed. When more SiO_2 is loaded, secondary aggregations of SiO_2 nanoparticles are gradually generated, and the size of SiO_2 cluster dramatically increases. The thermal/thermooxidative resistance and mechanical properties of NR/SiO_2 nanocomposites are compared to the NR host. The nanocomposites, particularly when the SiO_2 nanoparticles are uniformly dispersed, possess significantly enhanced thermal resistance and mechanical properties, which are strongly depended on the morphology of nanocomposites. The NR/SiO_2 has great potential to manufacture medical protective products with high performances.

Keywords: Natural rubber; Latex; Silica; Nanocomposite; Self-assembly

1. Introduction

Natural rubber (NR), one of the most important biosynthesized polymers displaying excellent chemical and physical properties, finds widely application in various areas [1–3]. Particularly, as an chemical-free biomacromolecule, natural rubber latex (NRL) has been used in manufacturing medical products such as medical gloves, condoms, blood transfusion tubing, catheters, injector closures and safety bags due to its excellent elasticity, flexibility, anti-virus permeation, good formability and biodegradability [4–6]. More recently, with the worldwide spread of the epidemic diseases such as acquired immure deficiency syndrome (AIDS), hepatitis B, severe acute respiratory syndrome (SARS) and avian influenza A (H5N1), it becomes increasingly important and urgent to develop high performance NRL protective products.

However, as its macromolecular backbone incorporates unsaturated cis-1,4-polyisoprenes, NR likes any other polymer is susceptible to oxidative or thermal degradation, particularly when formed into thin films. Once the degradation begins, NR readily becomes tacky and loses mechanical integrity. NRL products have, therefore, short shelf lives and life cycles. Though various anti-ageing agents have been successfully developed for dry NR products and limited anti-ageing agents for NRL were reported by using tris (nonylated phenyl) phosphite [7] and non-water-soluble

* Corresponding author. Address: Chinese Agricultural Ministry Key Laboratory of Natural Rubber Processing, Agricultural Product Processing Research Institute at Chinese Academy of Tropical Agricultural Sciences, Zhanjiang 524001, China. Tel.: +86 759 2286933; fax: +86 759 2221586.
E-mail address: zhengpeng8@yahoo.com (Z. Peng).

0266-3538/$ - see front matter © 2007 Elsevier Ltd. All rights reserved.
doi:10.1016/j.compscitech.2007.04.016

amino acids [8], no ideal anti-ageing agents have been identified so far for medical NRL products where strict safety and hygiene are required.

Low tensile strength and poor tear resistance are the other major drawbacks encountered in NRL products, especially for medical gloves and condoms. Attempts have been made to use carbon black [9], ultra-fine calcium carbonate [10], modified montmorillonite [11], silica [12] and starch [1] to reinforce dry NR or NRL. However, these traditional reinforcement materials are not so effective for NRL. Therefore, it is essential to exploit new way to enhance the ageing resistance and mechanical properties for NRL products.

Polymeric/inorganic nanocomposites (PINs) represent a radical alternative to conventional-filled polymers or polymer blends, and exhibit a controllable combination of the benefits of polymers (such as flexibility, toughness, and ease of processing) and those of inorganic phase (such as hardness, durability, and thermal stability) [13]. Such an improvement in combined characteristics is particularly significant at low loading levels of nano-fillers, which do not significantly increase the density of the compound or reduce light transmission. Therefore, introduction of inorganic nano-fillers into NR matrixes to overcome the aforementioned disadvantages of NR has recently attracted enormous interest. Most of these are using clay minerals with a unique multi-layered structure to reinforce NR via melt-intercalation [14,15], latex-compounding [16] and solution-mixing methods [17]. It was found that the organically modified clays with a loading up to 10 wt% have a good reinforcement on the NR matrix due to the intercalation/exfoliation of silicates and formation of a skeleton silicate network in NR matrix [15,16]. Nair et al. [18–20] also used nano crab chitin whiskers to reinforce NR. It was found that there is a three-dimensional chitin network within the NR matrix, which results in significantly improved solvent resistance and mechanical properties.

The high reinforcing efficiency of layered silicate rubber nanocompsites, even at low loading of layered silicates, is largely due to the nanoscale dispersion (the thickness of the layered silicates is 1 nm) and the very high aspect ratio of the silicate platelets (length-to-thickness ratio up to 2000). However, using fillers with higher specific surface such as spherical inorganic nanoparticles to directly reinforce NR, which has the potential to further improve the material properties, has not been reported. This is probably because there is no effective process to prevent the strong self-aggregation of nanoparticles.

In our previous work, a novel self-assembly nanocomposite process was developed to prepare a bulk polyvinyl alcohol/silica (PVA/SiO_2) nanocomposites [21–23]. We found that the chemical and physical properties of nanocomposites, compared to the polymer host, were significantly enhanced. The improvement in the properties is largely due to the uniform distribution of SiO_2 nanoparticles and the strong interactions between SiO_2 and polymer matrixes. We recently extended this self-assembly process to prepare NR/SiO_2 nanocomposites and briefly reported its preparation and thermal properties [24]. In the present paper, we will systematically discuss the self-assembly mechanism of the SiO_2 and NRL particles, observe the morphology of the nanocomposite and microstructure of SiO_2 nano-clusters with SEM and TEM, and investigate the impact of SiO_2 on thermal/thermooxidative resistance and mechanical properties.

2. Experimental section

2.1. Materials

Natural rubber latex (NRL) with a total solid content of 62% was purchased from Shenli Rubber Plantation (Zhanjiang, PR China), and was pre-vulcanised at room temperature for 2 days with the following formula: sulfur 1.5 parts per hundred rubber (phr); accelerator PX 1.2 phr; accelerator ZDC 0.8 phr; zinc oxide 1.5 phr; and an appropriate amount of stabiliser. Silica nanoparticles (average diameter: 14 nm; surface area: 200 m^2/g $\pm$ 25 m^2/g) and poly (diallyldimethylammonium chloride) (PDDA) (mol wt ca. 100,000–200,000; 20 wt% in water) were brought from Sigma–Aldrich (Sigma–Aldrich, Louis, MO). Water was Milli-Q water (18 MΩ-cm). All experimental materials were used as received.

2.2. Preparation of nanocomposite

In our previous work [24], we briefly reported a novel process to prepare NR/SiO_2 nanocomposites by combining latex-compounding and self-assembly techniques. Firstly, the negatively charged SiO_2 nanoparticles act as templates to adsorb positively charged PDDA molecular chains through electrostatic adsorption. Negatively charged NRL particles are then assembled onto the surface of SiO_2/PDDA nanoparticles. Finally, the SiO_2 nanoparticles are uniformly distributed in NR matrix. The key procedure of this process is the encapsulation of the SiO_2 nanoparticles with PDDA and NRL layers, aiming at suppressing the self-aggregation of SiO_2 nanoparticle caused by strong particle–particle interactions.

Specifically, the nanocomposites was prepared according to the following procedures. The SiO_2 nanoparticle aqueous dispersion of 1 wt% was treated with an ultrasonic vibrator for 0.5 h, and its pH was adjusted to 10 with 0.2 M NaOH to obtain negatively charged SiO_2 dispersion. A fixed amount of positively charged PDDA solution (pH 10) with a ratio of PDDA/SiO_2 = 5/100 w/w was then dropped into SiO_2 dispersion with mechanical stir. To remove PDDA that was not effectively absorbed on the surface of SiO_2 nanoparticles and avoid the flocculation of NRL particles cased by the redundant PDDA, the ultrasonically treated SiO_2/PDDA dispersion was centrifuged followed by rinsing with Milli-Q water. This step was repeated for 2 times. The rinsed SiO_2 particles were then collected and ultrasonically re-dispersed to obtain SiO_2/PDDA aqueous dispersion.

A fixed amount of NRL with a total solid content of 5% was treated with an ultrasonic vibrator for 0.5 h, and its pH was adjusted to 10 with 0.2 M NaOH to negatively charge the NRL particles. After that, the rinsed SiO_2/PDDA aqueous dispersion was then dropped into NRL with different mixture rates (NR/SiO_2 = 99.5/0.5, 99/1.0, 97.5/2.5, 96/4.0, 93.5/6.5 and 91.5/8.5 w/w) accompanying gentle mechanical stir at room temperature to obtain uniform NRL/SiO_2 dispersion, which was then dried in a vacuum oven at 50 °C to obtain NRL/SiO_2 nanocomposite films.

2.3. Characterizations

Scanning electron micrographs (SEM) of the nanocomposites were taken with a Philips XL 30 FEG-SEW instrument (Philips, Eindhoven, Netherlands) at an acceleration voltage of 10 kV. The fracture surface was obtained by splitting bulk sample being quenched in liquid nitrogen. A sputter coater was used to pre-coat conductive gold onto the fracture surface before observation. Thin films for transmission electron microscopy (TEM) were prepared by cutting bulk samples being quenched in liquid nitrogen. TEM observation was done on a JEM-100CXII instrument (JEOL, Peabody, MA) with an accelerating voltage of 100 KV.

A Perkin–Elmer TGA-7 thermogravimetric analyser (TGA) (Perkin–Elmer, Fremont, CA) was used for thermal and thermooxidative decomposition measurement. In nitrogen, the measurement of the films (ca. 10 mg) was carried out from 100 °C to 600 °C at a heating rate of 20 °C/min. In air, the TGA analysis was carried out from 100 °C to 700 °C at the same heating rate. The flow rate of the carrying gas is 80 ml/min. Fourier transform infrared spectroscopy (FTIR) was preformed on a Perkin–Elmer Spectra GX-I FTIR spectroscopy (Perkin–Elmer, Fremont, CA) with a resolution of 4 cm^{-1} in the transmission mode.

Tensile test and tear resistance experiments were conducted on an Instron Series IX Automated Materials Testing System (Instron, Acton, MA) with a cross head speed of 500 mm/min and the sample length between the jaws was 35 mm, the sample width 10 mm and the thickness 4.5 mm. The measurement was done at room temperature.

3. Results and discussion

3.1. Mechanism of self-assembly NR/SiO_2 nanocomposite process

When nanoparticles are dispersed with polymers, a core-shell structure tends to be formed in which nanoparticles covered with polymeric chains under certain conditions such as those used for self-assembly. By employing this approach, Caruso et al. [25] developed core-shell materials with given size, topology, and composition. Han and Armes [26] and Rotstein and Tannenbaum [27] studied polypyrrole, polystyrene and silica nanocomposites, respectively, and also confirmed the formation of this core-shell structure. In the present study, SiO_2 nanoparticles act as cores or templates to assemble PDDA and then adsorb NRL particles to develop a bulk NR/SiO_2 nanocomposite. There are two electrostatic adsorption stages in this process (Fig. 1) [24].

In the first stage, PDDA, an extensively used self-assembling material, is positively charged at the pH of 10 (Scheme 1) [28–30], and is adsorbed onto the surface of

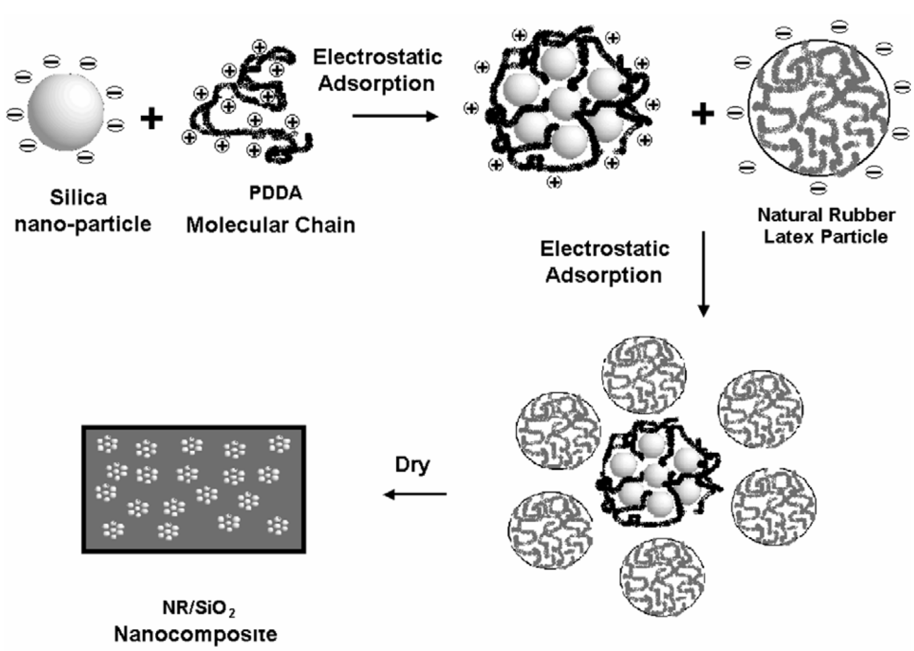

Fig. 1. The schematic of the self-assembly process [24].

negatively charged SiO_2 nanoparticles at the same pH (Scheme 2) by using the electrostatic adsorption as driving force. However, due to a large difference in rigidity between SiO_2 and PDDA and the charge density of PDDA is significantly larger than that on SiO_2, all of the former charges cannot form short-distance ion pairs with surface charges of rigid SiO_2 particles [30]. Therefore, the positive charge on PDDA cannot completely neutralized by the negative charge on SiO_2 particles during the assembly, and the SiO_2/PDDA core-shell particles will appear positive and be ready for next assembly with negatively charged NRL particles. To avoid the flocculation of NRL caused by the introduction of high molecular weight water-soluble cationic polyelectrolytes, PDDA that is not effectively assembled with SiO_2 is removed by the rinse presented in experimental section.

In the second assembly stage, the NRL particles are negatively charged as the protein particles adsorbed on the surface of the NRL particles contain carboxyl and amino functional groups (described as $P^{-\mathrm{COOH}}_{-\mathrm{NH_2}}$), which can be ionized in three different modes depending on pH value (Scheme 3). If the pH is lower than the isoelectric point of NRL (4.5–5.0), basic ionization will occur and NRL particles will be positively charged. Under isoelectric condition, NRL particles will remain neutral. As the pH used in the experiment (pH 10) is higher than the isoelectric point, acidic ionization is generated. NRL particles are, therefore, negatively charged. Again, under the drive of electrostatic adsorption, NRL particles are adsorbed onto the surface of SiO_2 particles that are covered with PDDA molecular chains in the previous assembly stage. Finally, the SiO_2 nanoparticles covered with PDDA and NRL layers are uniformly dispersed in NR matrix and dried (Fig. 1).

At the first assembly step, the SiO_2 nanoparticles act as the core of the SiO_2/PDDA core-shell structure. However, the core is not presented as individual SiO_2 nanoparticle, but as SiO_2 nano-cluster, which is evidenced by the SEM observation (Fig. 2), where the spherical nano-cluster and its primary structure unite: single nanoparticles can be clearly observed. This structure is also confirmed by the TEM image (Fig. 3), where the solid spherical SiO_2 nano-clusters with a diameter around 60 nm (presented as dark circle pies) are uniformly distributed in NR matrix.

According to Rotstein and Tannenbaum [27], the total number of SiO_2 primary nanoparticles in a cluster can be approximately estimated as

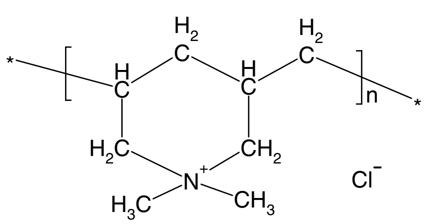

Scheme 1. Structure of PDDA at pH of 10.

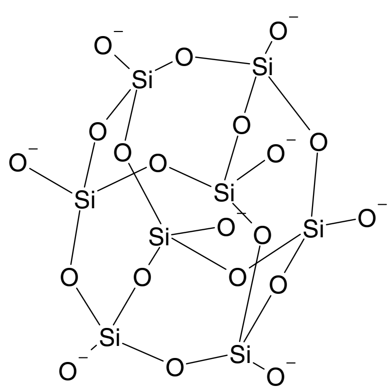

Scheme 2. Structure of SiO_2 at pH of 10.

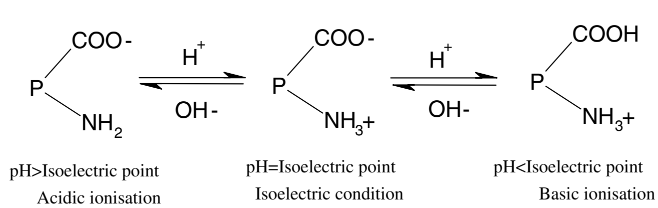

Scheme 3. Charge mechanism of the NRL particle.

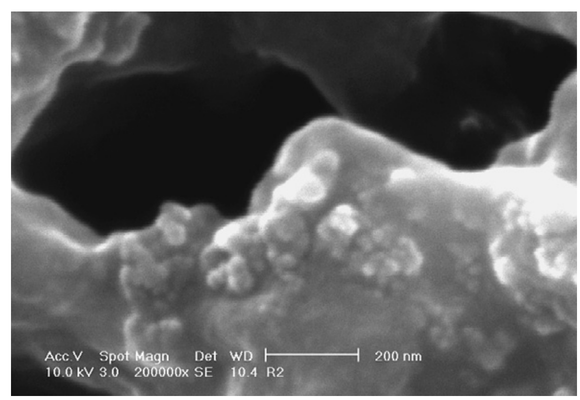

Fig. 2. SEM image of the nano-cluster (4 wt% SiO_2).

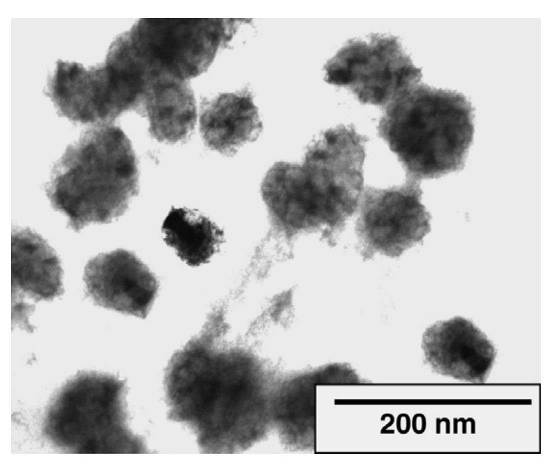

Fig. 3. TEM image of nano-cluster (4 wt% SiO_2).

$$N = \varepsilon \frac{\frac{4}{3}\pi R_2^3}{\frac{4}{3}\pi R_1^3} = \varepsilon \left(\frac{R_2}{R_1}\right)^3 \tag{1}$$

where N is the maximum number of SiO_2 nanoparticles in a cluster with a packing parameter, ε, of 1. R_1 is the radius of the SiO_2 nanoparticle (7 nm), and R_2 is the average radius of a cluster that is statistically measured from SEM images by using the following equation:

$$R_2 = \frac{\sum N_i \times R_i}{\sum N_i} \tag{2}$$

where N_i is the number of the clusters with radius R_i. The statistical information of the size distribution and the average radius is summarized in Table 1.

Combining Eqs (1) and (2), the average N for each nanocomposite can be obtained (Fig. 4). When a small amount of SiO_2 (0.5 wt%) is added, the N is around 80, while it gradually increases to 224 as the SiO_2 content increases to 4.0 wt%. It is clear that at low loadings the primary aggregations are generated. These primary aggregations are unlikely caused by the strong particle–particle interaction, but the adsorption between polymer molecular chain and SiO_2 nanoparticles, i.e. PDDA molecular chains adsorb quite a few separate nanoparticles to form nano-clusters in the stage of assembly. Therefore, the SiO_2 is not distributed in NR matrix as individual nanoparticles, but as nano-clusters. Similar assumption was found in polyethylene oxide (PEO)/silica nanocomposites. Gunb'ko et al. [31] reported that each PEO molecules could interact with many primary fumed SiO_2 particles to form small aggregates. We also observed this in the PVA/SiO_2 nanocomposites during the assembly between PVA and SiO_2 nanoparticles [21,23].

Table 1
Size distribution and average radius of SiO_2 cluster in NR matrix

NR/SiO_2	SiO_2 content (wt%)	Size distribution (nm)	Average radius (nm)
1	0.5	30–100	30
2	1.0	30–150	37.5
3	2.5	30–200	40
4	4.0	30–200	42.5
5	6.5	30–400	75
6	8.5	30–2500	–

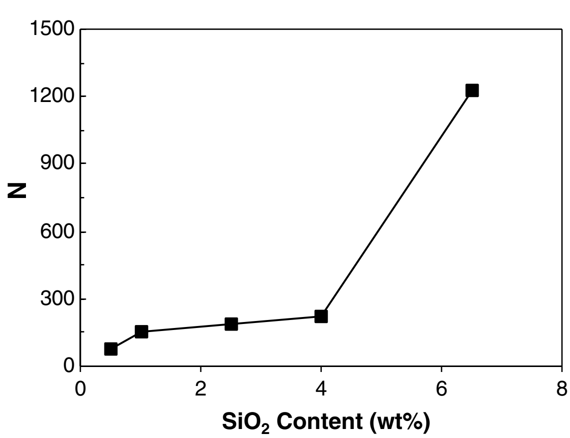

Fig. 4. The relationship between N and SiO_2 content.

However, a pronounced but interesting phenomenon has been observed: the nanoparticles aggregate greatly when the content of the SiO_2 nanoparticles is higher than 4 wt% (Fig. 8) and accordingly the size distribution of SiO_2 clusters increases significantly (Table 1). It is evident that secondary aggregations based on the primary aggregations are generated at high SiO_2 contents. A similar result was also found in PVA/SiO_2 nanocomposites where both primary and secondary aggregations were observed at a SiO2 content higher than 5 wt% [21,23]. However, without further information, we could not explain how and why the strong aggregation starts from this critical level. It will be investigated in our future work, as excessive particle aggregation will generally deteriorate the properties of the composites, and understanding the dispersion and aggregation mechanism during assembly is therefore critical for designing and synthesizing composites with stable behaviors.

3.2. Morphology of NR/SiO_2 nanocomposites

When the SiO_2 content is less than 4 wt%, almost all SiO_2 nanoparticles are homogenously distributed throughout the NR matrixes as individual spherical nano-clusters, but further increase in the SiO_2 content will lead to intensive aggregations. This can be observed from Fig. 5, which shows the morphology of the NR/SiO_2 nanocomposites with different SiO_2 contents. The dark phase represents the NR matrix and the bright phase corresponds to the SiO_2 particles, which are strongly embedded by NR matrix. The higher the SiO_2 content is, the more severe the aggregation can be observed. There is no obvious phase separation observed, implying the good miscibility between NR and SiO_2 that are treated with self-assembly process.

When only a very small amount of SiO_2 is added to the NR matrix (less than 1.0 wt%), most of the spherical clusters of nanoparticles are individually distributed amongst the NR matrixes (Fig. 5a). When more SiO_2 nanoparticles are loaded, the density of the SiO_2 clusters becomes higher. The SiO_2 clusters start aggregation in some areas for the nanocomposite with the SiO_2 content of 4 wt%, where the mixing is not appropriately done (Fig. 5b). When the SiO_2 is further increased to 6.5 wt%, the SiO_2 clusters are being aggregated in most areas. The aggregation dominates when the SiO_2 loading reaches 8.5 wt%. From the SEM micrograph with a lower magnification, the stratiform-like SiO_2 aggregation can be clearly observed (Fig. 5c).

From the statistical data, it can be seen that the size of the SiO_2 clusters has a very narrow distribution when the SiO_2 content is less than 4.0 wt% (Table 1). As more SiO_2 is added, the size distribution becomes significantly broader. Similarly, the average diameter of the SiO_2 clusters is quite stable (<85 nm) as SiO_2 is less than 4.0 wt%, it then markedly increases with the further addition of

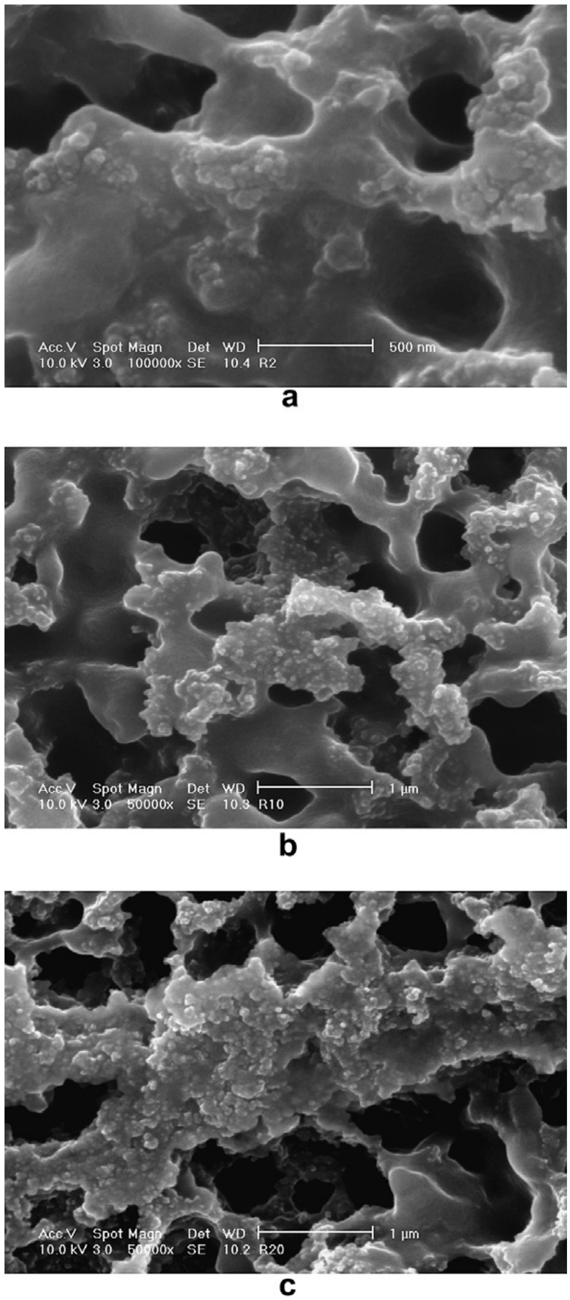

Fig. 5. SEM micrographs of NR/SiO_2 nanocomposites: (a) 1.0 wt% SiO_2, (b) 4.0 wt% SiO_2 and (c) 8.5 wt% SiO_2.

SiO_2. Fumed silica nanoparticles have been extensively used to prepare polymer/silica nanocomposites via melt compounding [32] and other physical blending [33]. However, silica has a number of hydroxyl groups on the surface, which results in the strong filler–filler or particle–particle interactions, and therefore has strong self-aggregation nature. In such conditions, the fumed SiO_2 nanoparticles tend to form loosely agglomerates that are dispersed with an average size in the range 300–400 nm, and these aggregated particles cannot be broken down by the shear forces during melt compounding [32]. Compared to other physical blending process, the process in the current work possesses significant advantages, as the size of SiO_2 is only around 85 nm.

3.3. FTIR study

Fourier transform infrared spectroscopy (FTIR) confirms the presence of SiO_2 in the NR host, and identifies the interaction between NR and SiO_2 phases. As presented in Fig. 6, in addition to the characterization peaks of NR at 1375 cm^{-1} and 835 cm^{-1}, the Si–O stretching vibration at 1100 cm^{-1} and bending vibration at 475 cm^{-1} [34,35] are also presented in the spectra of NR/SiO_2 nanocomposite, verifying the successful incorporation of the silica nanostructure into NR matrix. The shift of the peak at 3450 cm^{-1} was frequently used to study the hydrogen bonding between the –OH groups in the SiO_2 network and other functional groups from polymer molecular chains [36,37], and the shift of peak at the 1100 cm^{-1}, and the Si–O bending vibration at 476 cm^{-1} are the evidence of other interactions. Comparing to other polar rubber/silica systems [38,39], the above Si–O and –OH vibrating peak of SiO_2 shows a less significant shift. This means that the interaction between the NR macromolecular chains and SiO_2 is rather low when polar silica is distributed in the non-polar hydrocarbon rubber.

3.4. Thermal and thermooxidative ageing resistance

The thermal and thermooxidative ageing resistance of NR/SiO_2 nanocomposite can be assessed, respectively, from the investigation of thermal and thermooxidative decomposition. Fig. 7 are the TG and DTG curves of the pure NR and NR/SiO_2 nanocomposites in nitrogen. There is only one obvious thermal decomposition step of NR molecular chains, primarily initiated by thermal scissions of C–C chain bonds accompanying a transfer of hydrogen at the site of scission.

The thermooxidative decomposition is obviously different from the thermal decomposition as shown in Fig. 8, which are the TG and DTG curves of the pure NR and NR/SiO_2 nanocomposites in air, respectively. The first

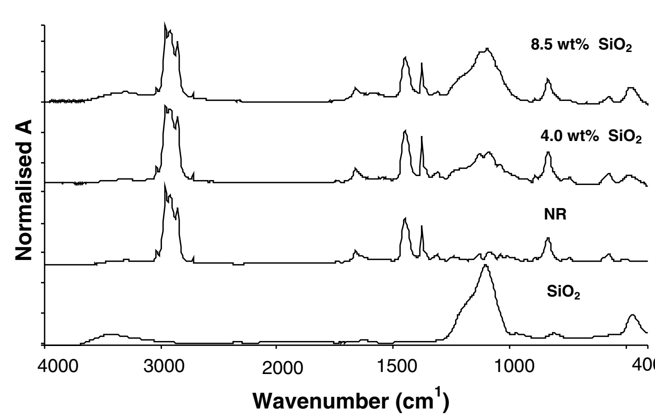

Fig. 6. FTIR spectra of SiO_2, NR and NR/SiO_2 nanocomposites.

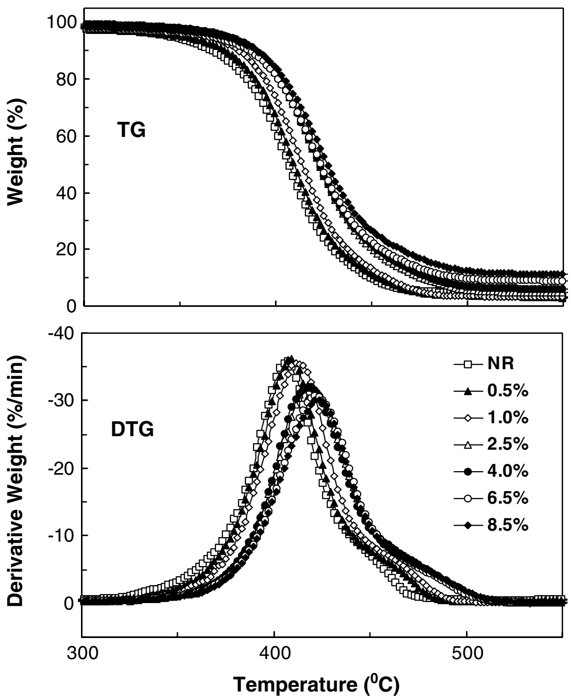

Fig. 7. TG curves for pure NR and NRL/SiO_2 nanocomposites in nitrogen.

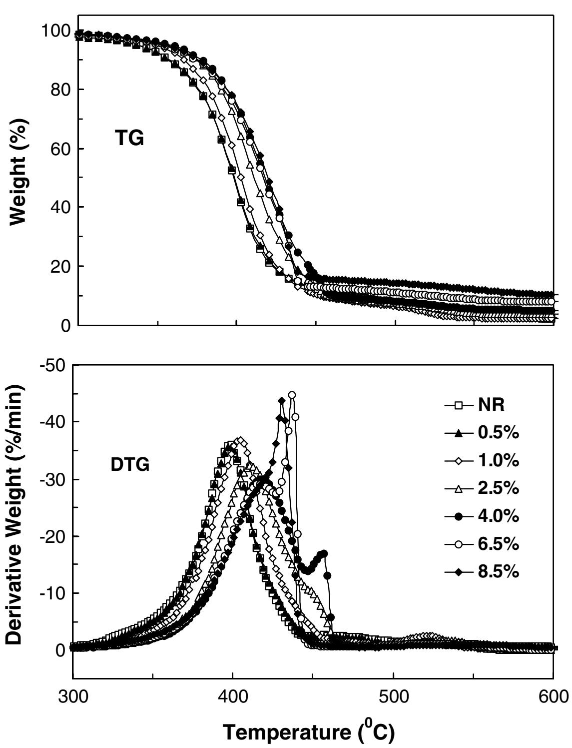

Fig. 8. DTG curves for pure NR and NRL/SiO_2 nanocomposites in air.

large decomposition peak is caused by oxidative dehydrogenation accompanying hydrogen abstraction, while the second weak peak is resulted from the oxidative reaction of residual carbon. When SiO_2 is introduced into NR matrix, the main decomposition peak shifts to a higher temperature and is gradually divided into two peaks. As more SiO_2 is added (>6.5 wt%), the side peak becomes sharper, suggesting that the thermooxidative decomposition of the NR/SiO_2 nanocomposites should be more complex than that of NR. However, without further information, the role of the SiO_2 in the thermooxidative decomposition of NR/SiO_2 nanocomposite is not clear. To reveal its thermal and thermooxidative decomposition mechanism, another investigation on thermal and thermooxidative decomposition of NR/SiO_2 using thermogravimetry-Fourier transform infrared spectroscopy (TG-FTIR), and pyrolysis-gas chromatography/massspectroscopy (Py-GC/MS) is being conducted and the results will be reported.

The DTG curve shows the maximum rate of weight loss, so the peak temperatures of decomposition (T_p) can be determined. The onset temperatures of decomposition (T_o) can be calculated from the TG curves by extrapolating from the curve at the peak of degradation back to the initial weight of the polymer. Similarly, the end temperature of degradation (T_f) can be calculated from the TG curves by extrapolating from the curve at the peak of degradation forward to the final weight of the polymer. The temperature range of the thermal degradation, an important parameter to evaluate the degree of degradation, is expressed as $\Delta T = T_p - T_o$. These characteristic temperatures are summarized in Table 2.

During thermal decomposition, T_o, T_p and T_f all increase with SiO_2 content and are relatively stable at the SiO_2 content of 4.0 wt%, where T_o, T_p and T_f of the NR/SiO_2 nanocomposites increase 10.4 °C, 10.3 °C and 12.2 °C compared to those of the pure NR, respectively.

Similar to the thermal decomposition, T_o, T_p and T_f of NR/SiO_2 nanocomposites during thermooxidative decomposition increase 13.6 °C, 21.9 °C and 22.7 °C at SiO_2 content of 4.0 wt%, in comparison with those of the pure NR, respectively. In addition, the ΔT for pure NR is smaller than that of the NR/SiO_2 nanocomposites, which means the chain scissions for the pure NR last for a shorter time. These significant increases in decomposition temperatures indicate that the thermal and thermooxidative ageing resistance of the NR/SiO_2 nanocomposite has been markedly improved.

The thermal and thermooxidative ageing resistance of prepared nanocomposite is dominated by the distribution of SiO_2 nanoparticles. Since the SiO_2 nanoparticles are homogenously distributed in NR matrix as nano-clusters when SiO_2 content is less than 4.0 wt%, the SiO_2 and NR molecular chains strongly interact through various effects such as the branching effect, nucleation effect, size effect, and surface effect. Therefore, the diffusion of decomposition products from the bulk polymer to gas phase is slowed down. Consequently, the nanocomposite has a more complex decomposition and a pronounced improvement of ageing resistance compared to the pure NR. With the further addition of SiO_2, the self-aggregation of SiO_2 is generated due to it being supersaturated and undoubtedly, the

Table 2
Characteristic temperatures of thermal and thermooxidative decomposition for pure NR and NR/SiO_2 nanocomposites with different SiO_2 contents

Sample	Thermal decomposition				Thermooxidative decomposition			
	T_o (°C)	T_p (°C)	T_f (°C)	ΔT (°C)	T_o (°C)	T_p (°C)	T_f (°C)	ΔT (°C)
NR	385.0	409.9	435.4	50.4	371.0	397.6	416.2	45.2
0.5%	386.1	411.1	436.8	50.7	371.6	397.6	417.8	46.2
1.0%	387.9	412.6	437.2	49.3	378.3	406.1	422.7	44.4
2.5%	392.6	417.8	444.8	52.2	382.3	414.6	436.0	53.7
4.0%	395.4	420.2	447.6	52.2	384.6	419.5	438.9	54.3
6.5%	396.0	421.1	448.8	52.8	385.1	432.2	440.9	55.8
8.5%	396.2	422.6	449.3	53.1	390.2	430.7	440.7	50.5

interaction density between SiO_2 and NR molecular chains decreases. Therefore, the ageing resistance of the nanocomposite cannot be further improved.

Another reason for the improvement in ageing resistance of NR/SiO_2 nanocomposites is that inorganic nanoparticles will migrate to the surface of the composites at elevated temperatures because of its relatively low surface potential energy [40]. This migration results in the formation of a SiO_2/NR char, which acts as a heating barrier to protect the NR inside. Similar result was found in Gilman [41] and Vyazovkin's [42] work where a clay/polymer char greatly enhances the thermal resistance of the host polymers.

3.5. Mechanical property

The incorporation of inorganic nanoparticles into elastomer matrix leads to a significant improvement in the mechanical properties of the host elastomer. Table 3 lists the mechanical properties of the pure NR and NR/SiO_2 nanocomposites with different SiO_2 loadings. NR, as a typical elastomer, shows an excellent flexibility and low rigidity. Because of the effective reinforcement of SiO_2, a dramatic improvement in the tensile strength is found as well as tensile modulus at different elongations. The elongation is just focused on 100%, 200% and 300%, as the filler–polymer interactions play a critical role at a low elongation, while at a high elongation the strain-reduced crystallisation of NR dominates the elongation [15]. The tensile strength and modules increase with the silica loading when less than 4 wt% SiO_2 is loaded. Even incorporating a small amount of SiO_2 (0.5 wt%) gives a remarkable enhancement in the tensile strength and modules, which reach a peak simultaneously at SiO_2 content of 4 wt%. However, with further addition of SiO_2, the tensile strength and modules gradually decrease due to SiO_2 aggregation.

Another noticeable improvement is observed in tear resistance. Poor tear resistance is one of the major problems for NRL product. Introducing SiO_2 into NR can significantly improve its tear resistance. The tear strength increases with an increasing SiO_2 loading. At SiO_2 content of 6.5 wt%, the tear strength (70.7 kN/m) is almost doubled that of the pure NR (37.1 kN/m). When inorganic nanofillers are homogenously distributed in polymer matrixes, they will macroscopically form an inorganic network, which mutually penetrates with polymer matrix and restricts the slides of polymer molecules, and therefore increases the mechanical properties of polymer hosts including tear resistance. However, the tear strength receives a significant decrease at the SiO_2 content of 8.5 wt%, as severe self-aggregation of SiO_2 are generated and the tear resistance of the NR host cannot increase but reduce.

However, the SiO_2 reduces the flexibility of NR due to the restriction in the molecular chain slipping along the filler surface. The influence of SiO_2 on NR's elongation at break seems relatively unnoticeable at low SiO_2 loading (less than 2.5 wt%), while it plays a critical role at high SiO_2. Particularly, the sample with the silica content of 8.5 wt% shows an extremely small elongation at break (384%) compared to that (995%) of the pure NR.

Similar to the thermal resistance, the improvement in various mechanical properties also shows a strong dependence on the morphology of composite. The better the SiO_2 dispersion, the better the properties of the nanocomposites as most of the mechanical properties peak at SiO_2 loading of 4 wt%, which is the turning point where heavy particle aggregations begin.

Table 3
Mechanical properties of pure NR and NR/SiO_2 nanocomposites

SiO_2 loading (wt%)	0	0.5	1.0	2.5	4.0	6.5	8.5
Tensile strength (Mpa)	15.1	18.0	19.8	22.7	26.3	21.0	1.06
Tensile modulus (Mpa)							
100% elongation	0.63	1.05	1.50	1.90	2.26	1.87	0.30
200% elongation	0.96	1.54	2.03	2.48	3.08	2.35	0.65
300% elongation	1.27	2.14	3.15	4.17	5.08	3.71	0.99
Elongation at break (%)	995	963	919	857	730	568	384
Tear strength (kN/m)	37.1	41.9	53.0	59.0	61.4	70.7	30.2

4. Conclusions

The self-assembly nanocomposite process has been successfully used to prepare a natural rubber/silica nanocomposite. When SiO_2 content is less than 4.0 wt%, by employing PDDA as an inter-medium, the SiO_2 nanoparticles are assembled with NRL particles as core-shell structure with slight primary aggregation, and the average size of SiO_2 nano-clusters is ranged from 60 to 85 nm. As more SiO_2 is loaded, heavy secondary aggregation of SiO_2 is gradually generated.

In comparison with pure NR, thermal and thermooxidative ageing resistances of prepared nanocomposite are significantly improved. During the thermal and thermooxidative decomposition, various characteristic temperatures of the NR/SiO_2 nanocomposites increase 10–25 °C over those of the pure NR.

The tensile strength, tensile modulus as well as tear strength of the resulting nanocomposite receive markedly increases at SiO_2 loadings of 2.5–4 wt%. The influence of SiO_2 on NR's flexibility is relatively samll at low SiO_2 loading, while it plays a critical role at high SiO_2 in reducing the elongation. The improvement in ageing resistances and mechanical properties are all dominated by the distribution of SiO_2 nanoparticles. The better the dispersion of SiO_2, the greater the improvement in the thermal and mechanical properties.

Acknowledgement

The financial support by the International Cooperation Project Foundation of Chinese Agricultural Ministry Key Laboratory of Natural Rubber Processing (Grant 706068 and 706069), is gratefully acknowledged.

References

[1] Angellier H, Molina-Boisseau S, Dufresne A. Mechanical properties of waxy maize starch nanocrystal reinforced natural rubber. Macromolecules 2005;38:9161–70.
[2] Sato S, Honda Y, Kuwahara M, Kishimoto H, Yagi N, Muraoka K, et al. Microbial scission of sulfide linkages in vulcanized natural rubber by a white rot basidiornycete, Ceriporiopsis subvermispora. Biomacromolecules 2004;5:511–5.
[3] Sanguansap K, Suteewong T, Saendee P, Buranabunya U, Tangboriboonrat P. Composite natural rubber based latex particles: a novel approach. Polymer 2005;46:1373–8.
[4] Bode HB, Kerkhoff K, Jendrossek D. Bacterial degradation of natural and synthetic rubber. Biomacromolecules 2001;2:295–303.
[5] Schwerin M, Walsh D, Richardson D, Kisielewski R, Kotz R, Routson L, et al. Biaxial flex-fatigue and viral penetration of natural rubber latex gloves before and after artificial aging. J Biomed Mater Res 2002;63:739–45.
[6] Walsh DL, Schwerin MR, Kisielewski RW, Kotz RM, Chaput MP, Varney GW, et al. Abrasion resistance of medical glove materials. J Biomed Mater Res B 2004;68:81–7.
[7] Kurian JK, Peethambaran NR, Mary KC, Kuriakose B. Effect of vulcanization systems and antioxidants on discoloration and degradation of natural rubber latex thread under UV radiation. J Appl Polym Sci 2000;78:304–10.
[8] Abad L, Relleve L, Aranilla C, Aliganga A, Diego CS, Rosa AD. Natural antioxidants for radiation vulcanization of natural rubber latex. Polym Degrad Stabil 2002;76:275–9.
[9] Busfield JJC, Deeprasertkul C, Thomas AG. The effect of liquids on the dynamic properties of carbon black filled natural rubber as a function of pre-strain. Polymer 2000;41:9219–25.
[10] Cai HH, Li SD, Rian TG, Wang HB, Wang JH. Reinforcement of natural rubber latex film by ultrafine calcium carbonate. J Appl Polym Sci 2003;87:982–5.
[11] Arroyo M, Lopez-Manchado MA, Herrero B. Organo-montmorillonite as substitute of carbon black in natural rubber compounds. Polymer 2003;44:2447–53.
[12] Jose L, Joseph R. Study of the effect of polyethylene-glycol in field natural-rubber latex vulcanizates. Kaut Gummi Kunstst 1993;46:220–2.
[13] Kong LX, Peng Z, Li SD, Bartold PM. Nanotechnology and its role in the management of periodontal diseases. Periodontol 2000 2006;40:184–96.
[14] Teh PL, Ishak ZAM, Hashim AS, Karger-Kocsis J, Ishiaku US. Effects of epoxidized natural rubber as a compatibilizer in melt compounded natural rubber-organoclay nanocomposites. Eur Polym J 2004;40:2513–21.
[15] Varghese S, Karger-Kocsis J. Melt-compounded natural rubber nanocomposites with pristine and organophilic layered silicates of natural and synthetic origin. J Appl Polym Sci 2004;91:813–9.
[16] Varghese S, Karger-Kocsis J. Natural rubber-based nanocomposites by latex compounding with layered silicates. Polymer 2003;44:4921–7.
[17] Magaraphan R, Thaijaroen W, Lim-Ochakun R. Structure and properties of natural rubber and modified montmorillonite nanocomposites. Rubber Chem Technol 2003;76:406–18.
[18] Nair KG, Dufresne A. Crab shell chitin whisker reinforced natural rubber nanocomposites. 1. Processing and swelling behavior. Biomacromolecules 2003;4:657–65.
[19] Nair KG, Dufresne A. Crab shell chitin whisker reinforced natural rubber nanocomposites. 2. Mechanical behavior. Biomacromolecules 2003;4:666–74.
[20] Nair KG, Dufresne A, Gandini A, Belgacem MN. Crab shell chitin whiskers reinforced natural rubber nanocomposites. 3. Effect of chemical modification of chitin whiskers. Biomacromolecules 2003;4:1835–42.
[21] Peng Z, Kong LX, Li SD. Non-isothermal crystallisation kinetics of self-assembled polyvinylalcohol/silica nano-composite. Polymer 2005;46:1949–55.
[22] Peng Z, Kong LX, Li SD. Thermal properties and morphology of poly (vinyl alcohol)/silica nanocomposite prepared with self-assembled monolayer technique. J Appl Polym Sci 2005;96:1436–42.
[23] Peng Z, Kong LX, Li SD, Spiridonov P. Polyvinyl alcohol/Silica nanocomposite: its morphology and thermal degradation kinetics. J Nanosci Nanotechnol 2006;6:3934–8.
[24] Li SD, Peng Z, Kong LX, Zhong JP. Thermal degradation kinetics and morphology of natural rubber/silica nanocomposites. J Nanosci Nanotechno 2006;6:541–6.
[25] Caruso F, Caruso RA, Mohwald H. Nanoengineering of inorganic and hybrid hollow spheres by colloidal templating. Science 1998;282:1111–4.
[26] Han MG, Armes SP. Preparation and characterization of polypyrrole–silica colloidal nanocomposites in water–methanol mixtures. J Colloid Interf Sci 2003;262:418–27.
[27] Rotstein H, Tannenbaum R. In: Baraton M-I, editor. Synthesis, functionalization and surface treatment of nanoparticles. Stevenson Ranch: American Scientific Publishers; 2003. p. 103–26.
[28] Cassagneau T, Guerin F, Fendler JH. Preparation and characterization of ultrathin films layer-by-layer self-assembled from graphite oxide nanoplatelets and polymers. Langmuir 2000;16:7318–24.
[29] Katagiri K, Caruso F. Functionalization of colloids with robust inorganic-based lipid coatings. Macromolecules 2004;37:9947–53.

[30] Lvov Y, Ariga K, Onda M, Ichinose I, Kunitake T. Alternate assembly of ordered multilayers of SiO2 and other nanoparticles and polyions. Langmuir 1997;13:6195–203.
[31] Gun'ko VM, Zarko VI, Leboda R, Chibowski E. Aqueous suspension of fumed oxides: particle size distribution and zeta potential. Adv Colloid Interfac 2001;91:1–112.
[32] Kim SH, Ahn SH, Hirai T. Crystallization kinetics and nucleation activity of silica nanoparticle-filled poly(ethylene 2,6-naphthalate). Polymer 2003;44:5625–34.
[33] Merkel TC, Freeman BD, Spontak RJ, He Z, Pinnau I, Meakin P, et al. Ultrapermeable, reverse-selective nanocomposite membranes. Science 2002;296:519–22.
[34] Saito R, Tobe T. Electrical properties of poly(2-vinyl pyridine)/silica nanocomposites prepared with perhydropolysilazane. Polym Adv Technol 2005;16:232–8.
[35] Shen L, Zhong W, Wang HT, Du QG, Yang YL. Preparation and characterization of SMA(SAN)/silica hybrids derived from water glass. J Appl Polym Sci 2004;93:2289–96.
[36] Chen X, Wu L, Zhou S, You B. In situ polymerization and characterization of polyester-based polyurethane/nano-silica composites. Polym Int 2003;52:993–8.
[37] Tong X, Tang T, Zhang Q, Feng Z, Huang B. Polymer/silica nanoscale hybrids through sol–gel method involving emulsion polymers. I. Morphology of poly(butyl methacrylate)/SiO2. J Appl Polym Sci 2002;83:446–54.
[38] Glime J, Koenig JL. FTIR investigation of the molecular structure at the crack interface in unfilled and silica filled polyisoprene. Rubber Chem Technol 2000;73:47–55.
[39] Varghese S, Gatos KG, Apostolov AA, Karger-Kocsis J. Morphology and mechanical properties of layered silicate reinforced natural and polyurethane rubber blends produced by latex compounding. J Appl Polym Sci 2004;92:543–51.
[40] Marosi G, Marton A, Szep A, Csontos I, Keszei S, Zimonyi E, et al. Fire retardancy effect of migration in polypropylene nanocomposites induced by modified interlayer. Polym Degrad Stabil 2003;82:379–85.
[41] Gilman JW, Jackson CL, Morgan AB, Harris R, Manias E, Giannelis EP, et al. Chem Mater 2000;12:1866–73.
[42] Vyazovkin S, Dranca I, Fan XW, Advincula R. Kinetics of the thermal and thermo-oxidative degradation of a polystyrene–clay nanocomposite. Macromol Rapid Commun 2004;25: 498–503.